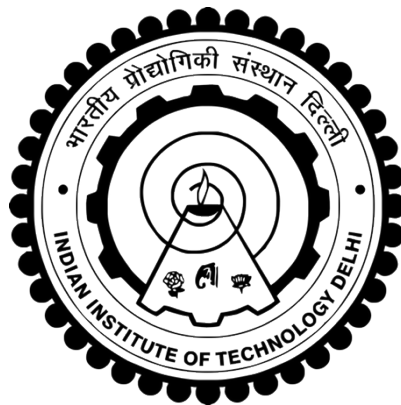


**BIO-MEDICAL DIAGNOSIS OF BONES THROUGH
COLLOCATED ACTION OF SHAPE MEMORY ALLOY
(SMA) ACTUATORS AND PIEZO SENSORS**

SHASHANK SRIVASTAVA



**DEPARTMENT OF CIVIL ENGINEERING
INDIAN INSTITUTE OF TECHNOLOGY DELHI
JUNE 2018**

© Indian Institute of Technology Delhi (IITD), New Delhi, 2018

**BIO-MEDICAL DIAGNOSIS OF BONES THROUGH
COLLOCATED ACTION OF SHAPE MEMORY ALLOY
(SMA) ACTUATORS AND PIEZO SENSORS**

by

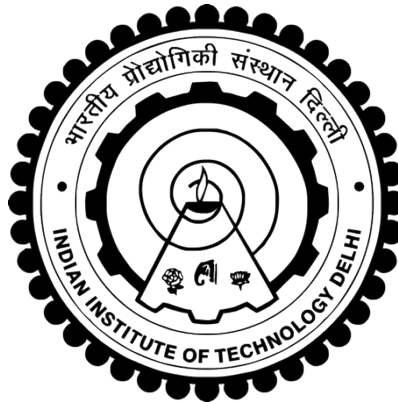
SHASHANK SRIVASTAVA

Department of Civil Engineering

Submitted

in fulfilment of the requirements of the degree of doctor of philosophy

to the



INDIAN INSTITUTE OF TECHNOLOGY DELHI

JUNE 2018

*Dedicated to my spiritual master H.H. Gopal Krsna Goswami and
my parents*

CERTIFICATE

This is to certify that the thesis entitled, “**BIO-MEDICAL DIAGNOSIS OF BONES THROUGH COLLOCATED ACTION OF SHAPE MEMORY ALLOY (SMA) ACTUATORS AND PIEZO SENSORS**” submitted by **Mr. Shashank Srivastava** to Indian Institute of Technology Delhi, for the award of the degree of the **Doctor of Philosophy** is a record of bonafide research work carried out by him. He worked under our supervision for the submission of this thesis, which to the best of our knowledge has reached the requisite standard.

The research reports and the results presented in this thesis have not been submitted in parts or in full to any other University or Institute for the award of any degree or diploma.

(Prof. Suresh Bhalla)

Professor

Department of Civil

Engineering

Indian Institute of

Technology Delhi

(Prof. Alok Madan)

Professor

Department of Civil

Engineering

Indian Institute of

Technology Delhi

(Prof. Ashok Gupta)

Professor

Department of Civil

Engineering

Indian Institute of

Technology Delhi

ACKNOWLEDGEMENTS

First and foremost I express my heartfelt gratitude towards my supervisors, Prof. Suresh Bhalla, Prof. Alok Madan and Prof. Ashok Gupta for their continuous guidance, encouragement and advice during the course of my Ph.D. research. I am forever grateful for their kindness and contributions both for my research and my professional development.

I am also grateful to other members of Prof. Bhalla's research team namely Mr. Sumit, Dr. T. Visalakshi , Dr. Sumedha Moharana, Dr. Naveet Kaur and Mr.S.K. Dhawan who were always there to support in all possible ways. Thanks are also due to technicians, Mr. Lal Singh, Mr. Vinod Sharma, Mr. Dharmendra Singh and Mr. Devender Kumar who assisted in performing many of the experiments by providing good technical support. All the experimental work went smoothly due to their support and good environment in the Smart Structures and Dynamics Laboratory. I am also thankful to my colleagues Prof. Subhasish Maji , Mrs. Shweta Tripathi and Dr. Sanjay Agrawal who were instrumental in encouraging me to go for Phd research and to Dr. Venkat and Dr. Rakhi Sharma who always motivated me for swift completion of work.

I am always indebted to my parents and my sister for their encouragement and sacrifices and special thanks to my wife, who managed the household work very nicely and provided me with ample time for my Ph.D. work. Special thanks to my newly born son, Master Madhavendra, who provided enough relaxation during thesis writing work.

Shashank Srivastava

ABSTRACT

During past few years, tremendous research efforts have been undertaken for the integration of smart materials in the fields of bio-mechanics and bio-medical engineering. Smart materials, being miniature in size and shape and also light weight, are the best candidates for bio-medical structural health monitoring (BSHM). Development of non-invasive techniques for long-term and continuous monitoring of critical organs has recently become a major area of interest to a large number of academic and medical laboratories. The associated techniques strive to achieve a quick health monitoring of bio-medical subjects with minimum hazards.

This thesis focuses on developing a new diagnostic technique for non-invasive detection of fractures and physiological decay such as osteomalacia and osteoporosis using lead zirconate titanate (PZT) patches in the framework of the electro-mechanical impedance (EMI) technique in combination with shape memory alloys (SMA). The basic principle behind the EMI technique is to employ high frequencies (typically >30 kHz), generated by a surface-bonded PZT patch, to detect changes in the structural drive point impedance caused by any damage such as internal/ surface cracks, loose connections, delaminations etc. The resultant electro-mechanical interaction, which is characteristic of the particular structure, modulates the current flowing through the PZT patch. The modulation is a function of the degree of mechanical interaction between the patch and the host structure over the selected frequency range. The resultant admittance signature, which acts like a frequency response function (FRF), is employed as a ‘fingerprint’ of the structural system for the purpose of damage diagnosis. Any changes occurring in the admittance signature provides an indication of any damage occurring in the host structure.

Despite the undisputed success of the EMI technique for most routine engineering related structural health monitoring (SHM), the adhesive bonding of the PZT patch on the host structure has been a major limitation to its full-fledged application for BSHM. Bonding a piezo patch onto the skin of a live subject is not only a cause of irritation for the subject but may also result in skin disease and serious injury. In the past, researchers have successfully demonstrated the effectiveness of bonded piezo patch for crack detection and healing of bones. Development of suitable experimental methodology for employing PZT patches in non-bonded mode shall definitely alleviate this major limitation prohibiting the EMI technique for BSHM.

The main objective of the research work covered in this thesis has been to develop a proof-of-concept non-bonded piezo sensor (NBPS) configuration apt for EMI technique based BSHM. To meet this objective, shape memory alloy (SMA) wires have been employed to secure the NBPS configuration on a live subject in an autonomous fashion so as to circumvent mechanical clamping. As the first step, experimental investigations on human hand bone replica made of polyvinyl chloride (PVC) were carried out using mechanical clamping. The effectiveness of the NBPS was gauged at three different levels of clamp tightening using jubilee clamps. The requisite circumferential strain was established through comparison with conductance signatures resulting from directly bonded piezo sensor (DBPS). Thereafter, physiological damage in the bone was induced and detailed investigations carried out to correlate the changes in the NBPS based conductance signature with damage. Two more bone models resembling femur in humans were then investigated to establish adequacy of the NBPS configuration for diagnosis of osteoporosis. Experiments also established the feasibility of determining the density/Young's modulus of the osteoporotic bone from the current signature, thus circumventing

the necessity of acquiring the baseline signature. The effectiveness of the NBPS configuration in the presence of skin layer, which is an indispensable requirement, was successfully carried out using silicon layer over the experimental bone as skin. The proposed configuration was finally successfully tested on a human subject also.

This mechanical bonding, though improvement over adhesive bonding, could still be a cause of discomfort and also impose practical limitations. To circumvent this limitation, proof-of-concept demonstration of automatic reversible clamping using SMAs was finally established vis-a-vis the mechanically clamped configuration. Parametric evaluation of bone deterioration based on extracted equivalent stiffness parameter (ESP) was also successfully established. A numerical model of the NBPS and DBPS based piezo-bone system was developed using PZFlex finite element modelling (FEM) platform. After validation with experimental results, the FEM model was employed for parametric investigations aiming for better application of the NBPS configuration in real-life.

To the candidate's best knowledge, this is the first ever proof-of-concept experimental development towards achieving NBPS configuration for EMI technique using SMA in the field of BSHM. Proposed NBPS configuration and related investigation shall have significant ramifications in the BSHM sector.

सार

पिछले कुछ वर्षों के दौरान जैव-मैकेनिक्स और बायो-मेडिकल इंजीनियरिंग के क्षेत्र में स्मार्ट सामग्री के एकीकरण के लिए जबरदस्त अनुसंधान प्रयास किए गए हैं। लघु आकार और हल्के वजन के होने के कारण, स्मार्ट सामग्री जैव-चिकित्सा संरचनात्मक स्वास्थ्य निगरानी (बीएसएचएम) के लिए सर्वश्रेष्ठ उम्मीदवार है। दीर्घकालिक और महत्वपूर्ण अंगों की निरंतर निगरानी के लिए नान-इनवेसिव तकनीकों का विकास हाल ही में अकादमिक और चिकित्सा प्रयोगशालाओं की बड़ी संख्या में रुचि का एक प्रमुख क्षेत्र बन गया है। संबंधित तकनीक न्यूनतम खतरों वाले जैव-चिकित्सा विषयों की त्वरित स्वास्थ्य निगरानी प्राप्त करने का प्रयास करती है।

यह थीसिस फ्रैक्चर और शारीरिक क्षय जैसे ओस्टियोमालेशिया और ओस्टियोपोरोसिस की नान-इनवेसिव पहचान इलेक्ट्रो-मैकेनिकल प्रतिबाधा (ईएमआई) तकनीक के ढांचे में, लीड ज़िकॉनेट टाइटेनेट (पीजेडटी) पैच एवं आकार मेमोरी मिश्र धातु (एसएमए) के संयोजन का उपयोग करते हुए एक नई नैदानिक तकनीक विकसित करने पर केंद्रित है। ईएमआई तकनीक के पीछे मूल सिद्धांत उच्च आवृत्तियों (आमतौर पर > 30 केएचजेड) को नियोजित करना है, जो सतह-बंधुआ पीजेडटी पैच द्वारा उत्पन्न होता है और आंतरिक सतह दरारों, ढीले कनेक्शन, गैर-परतबंदी, इत्यादि जैसे किसी भी नुकसान के कारण संरचनात्मक ड्राइव बिंदु प्रतिबाधा में परिवर्तन का पता लगाता है। परिणामी इलेक्ट्रो-मैकेनिकल इंटरैक्शन, जो कि विशेष संरचना की विशेषता है, वर्तमान में पीजेडटी पैच के माध्यम से बहती धारा को संशोधित करता है। मॉड्यूलेशन, पैच और मेजबान संरचना के बीच चयनित आवृत्ति रेंज पर मैकेनिकल इंटरैक्शन की डिग्री का एक कार्य है। परिणामस्वरूप प्रवेश हस्ताक्षर, जो आवृत्ति प्रतिक्रिया फंक्शन (एफआरएफ) की तरह कार्य करता है, क्षति निदान के उद्देश्य के लिए संरचनात्मक प्रणाली के 'फिंगरप्रिंट' के रूप में कार्यरत है। प्रवेश हस्ताक्षर में होने वाले कोई भी परिवर्तन मेजबान संरचना में होने वाले किसी भी नुकसान का संकेत प्रदान करता है।

अधिकांश नियमित इंजीनियरिंग से संबंधित संरचनात्मक स्वास्थ्य निगरानी (एसएचएम) के लिए ईएमआई तकनीक की निर्विवाद सफलता के बावजूद, मेजबान संरचना पर पीजेडटी पैच का चिपकने वाला बंधन बीएसएचएम के लिए उसके पूर्ण उपयोग के लिए एक प्रमुख बाधा

रहा है। एक जीवित विषय की त्वचा पर एक पीजो पैच को बांधना न केवल विषय के लिए जलन का कारण है बल्कि त्वचा की बीमारी और गंभीर चोट भी कर सकता है। अतीत में, शोधकर्ताओं ने क्रैक का पता लगाने और हड्डियों के उपचार के लिए बंधुआ पीजो पैच की प्रभावशीलता का सफलतापूर्वक प्रदर्शन किया है । गैर-बंधन मोड में पीजेडटी पैच को नियोजित करने के लिए उपयुक्त प्रयोगात्मक पद्धति का विकास निश्चित रूप से बीएसएचएम के लिए ईएमआई तकनीक को प्रतिबंधित करने वाली इस प्रमुख बाधा को कम करेगा।

इस शोध में शामिल किए गए अनुसंधान कार्य का मुख्य उद्देश्य एक सबूत अवधारणा-का-गैर बंधुआ पीजो सेंसर (एनबीपीएस) विन्यास विकसित करना है जो कि ईएमआई आधारित बीएसएचएम तकनीक के लिए उपयुक्त हो । इस उद्देश्य को पूरा करने के लिए, यांत्रिक क्लैम्पिंग को रोक कर एक स्वायत्त फैशन में लाइव विषय पर एनबीपीएस कॉन्फिगरेशन को मेमोरी मिश्र धातु (एसएमए) तारों द्वारा सुरक्षित किया गया है। पहले चरण के रूप में, पॉलीविनाइल क्लोराइड (पीवीसी) से बने मानव हाथ की हड्डी प्रतिकृति पर प्रयोगात्मक जांच यांत्रिक क्लैम्पिंग का उपयोग करके की जाती थी। जुबिली क्लैप का उपयोग करके क्लैप कसने के तीन अलग-अलग स्तरों पर एनबीपीएस की प्रभावशीलता का अनुमान लगाया गया था। अपेक्षित परिधीय तनाव सीधे बंधुआ पीजो सेंसर (डीबीपीएस) से उत्पन्न प्रवाहकत्व हस्ताक्षर के साथ तुलना के माध्यम से स्थापित किया गया था। इसके बाद, हड्डी में शारीरिक क्षति को प्रेरित किया गया और क्षति के साथ एनबीपीएस आधारित प्रवाहकत्व हस्ताक्षर में परिवर्तनों को सहसंबंधित करने के लिए विस्तृत जांच की गई। मनुष्यों में फीमर जैसी दो और हड्डी मॉडल की जांच ऑस्टियोपोरोसिस के निदान हेतु एनबीपीएस कॉन्फिगरेशन की पर्याप्तता स्थापित करने के लिए की गई। प्रयोगों ने वर्तमान हस्ताक्षर से ऑस्टियोपोरोटिक हड्डी के घनत्व / यंग मॉड्यूलस को निर्धारित करने की व्यवहार्यता भी स्थापित की, इस प्रकार बेसलाइन हस्ताक्षर प्राप्त करने की आवश्यकता को दरकिनार कर दिया। त्वचा परत की उपस्थिति में एनबीपीएस कॉन्फिगरेशन की प्रभावशीलता, जो एक अनिवार्य आवश्यकता है, प्रयोगात्मक हड्डी पर त्वचा के रूप में सिलिकॉन परत का उपयोग करके सफलतापूर्वक किया गया। प्रस्तावित विन्यास का अंततः मानव विषय पर भी सफलतापूर्वक परीक्षण किया गया ।

यह यांत्रिक बंधन, हालांकि चिपकने वाले बंधन से सुधारात्मक होते हुए भी असुविधा का कारण हो सकता है और व्यावहारिक सीमाएं भी लगा सकता है। इस सीमा को रोकने के

लिए, एसएमए का उपयोग कर स्वचालित रिवर्सिबल क्लैपिंग का सबूत-अवधारणा प्रदर्शन अंततः मैकेनिकल क्लैम्पड कॉन्फ़िगरेशन के साथ स्थापित किया गया था । निकाले गए समतुल्य कठोरता पैरामीटर (ईएसपी) के आधार पर हड्डी में क्षय का पैरामेट्रिक मूल्यांकन भी सफलतापूर्वक स्थापित किया गया । एनबीपीएस और डीबीपीएस आधारित पीजो-हड्डी प्रणाली का एक संख्यात्मक मॉडल का उपयोग कर पीजेडफ़्लेक्स सॉफ्टवेयर मंच पर परिमित तत्व मॉडलिंग (एफईएम) विकसित किया गया। प्रयोगात्मक परिणामों के सत्यापन के बाद, एफईएम मॉडल को वास्तविक जीवन में एन.बी.पी.एस कॉन्फ़िगरेशन के बेहतर सदुपयोग के उद्देश्य से पैरामीट्रिक जांच के लिए नियोजित किया गया था।

उम्मीदवार की सर्वोत्तम जानकारी में, यह बीएसएचएम के क्षेत्र में एसएमए का उपयोग करते हुए ईएमआई तकनीक द्वारा एनबीपीएस कॉन्फ़िगरेशन प्राप्त करने की दिशा में पहला सबूत-अवधारणा प्रयोगात्मक विकास है। प्रस्तावित एनबीपीएस विन्यास और संबंधित जांच , बीएसएचएम के क्षेत्र में महत्वपूर्ण असर डालेगा ।

Table of Contents

CERTIFICATE	i
ACKNOWLEDGEMENTS.....	ii
ABSTRACT	iii
TABLE OF CONTENTS.....	vi
LIST OF FIGURES.....	ix
LIST OF TABLES.....	xv
LIST OF SYMBOLS.....	xvi
LIST OF ACRONYMS.....	xviii
Chapter 1 INTRODUCTION	1
1.1 BACKGROUND	1
1.2 RESEARCH OBJECTIVES AND SCOPE	4
1.3 ORGANIZATION OF THESIS	5
Chapter 2 SMART MATERIALS FOR BSHM AND MEDICAL DIAGNOSTICS	6
2.1 INTRODUCTION	6
2.2 CONVENTIONAL SENSING TECHNIQUES AND SENSORS FOR BSHM	6
2.3 SMART MATERIALS IN BSHM	10
2.3.1 Optical Fibres.....	11
2.3.2 Piezoelectric Sensors	13
2.3.3 Shape Memory Alloys (SMA).....	16
2.4 ELECTRO-MECHANICAL IMPEDANCE (EMI) TECHNIQUE	23
2.5 BIO-MEDICAL APPLICATIONS OF EMI TECHNIQUE	26
2.6 IDENTIFICATION OF GAPS	29
2.7 RESEARCH OBJECTIVES	29
2.8 CONCLUDING REMARKS.....	30
Chapter 3 PROOF-OF-CONCEPT DEVELOPMENT OF NON-BONDED PIEZO CONFIGURATION	31
3.1 INTRODUCTION	31
3.2 NON-BONDED EXPERIMENTAL CONFIGURATION FOR PULSE RATE MEASUREMENT (SENSOR EFFECT)	31
3.3 EXPERIMENTAL NON-BONDED CONFIGURATION FOR EMI TECHNIQUE (SENSOR-ACTUATOR EFFECT).....	35
3.3.1 Preliminary Investigations	35
3.3.2 Development of Improved Clamping for NBPS	39
3.4 CONCLUDING REMARKS.....	42
Chapter 4 DEVELOPMENT OF EVALUATION OF NBPS CONFIGURATION FOR BIO-MEDICAL SUBJECTS.....	43
4.1 INTRODUCTION	43
4.2 EXTENSION OF NBPS CONFIGURATION TO BONES	44
4.3 OPTIMIZATION OF CLAMP TIGHTENING STRAIN.....	46
4.4 NBPS CONFIGURATION FOR MONITORING BONE DEGRADATION	53

4.5 IDENTIFICATION OF OSTEOPOROTIC CONDITION	56
4.6 EXTENSION OF NBPS CONFIGURATION FOR BONE COVERED WITH SKIN	61
4.7 EXTENSION OF NBPS ON LIVE SUBJECT	67
4.8 CONCLUDING REMARKS.....	69
Chapter 5 GRIP AUTOMATION OF NBPS USING SHAPE MEMORY ALLOY WIRES	70
5.1 INTRODUCTION	70
5.2 EXPERIMENTAL METHODOLOGY FOR NBPS GRIP AUTOMATION.....	70
5.3 CALCULATIONS FOR DETERMINING THE LENGTH OF SMA WIRE REQUIRED FOR NBPS GRIP	72
5.4 RESULTS	73
5.5 CONCLUDING REMARKS.....	74
Chapter 6 IMPEDANCE BASED IDENTIFICATION AND DIAGNOSIS USING NBPS	78
6.1 INTRODUCTION	78
6.2 ELECTRICAL AND MECHANICAL SYSTEMS ANALOGY	78
6.3 METHODOLOGY AND PHYSICAL INTERPRETATION	80
6.4 IMPEDANCE BASED IDENTIFICATION FOR EXPERIMENTAL BONES	83
6.4.1 Healthy and Osteoporotic Femurs	83
6.4.2 Hand Bone	87
6.5 QUANTIFICATION OF NBPS CLAMPING	90
6.6 CONCLUDING REMARKS.....	90
Chapter 7 NUMERICAL PARAMETRIC STUDY INVESTIGATIONS ON NBPS CONFIGURATION	91
7.1 INTRODUCTION	91
7.2 DEVELOPMENT OF NUMERICAL MODEL AND COMPUTATIONAL METHODOLOGY	92
7.3 MODEL VALIDATION	96
7.4 SIMULATION OF NBPS CLAMPING PROCEDURE.....	99
7.5 PARAMETRIC STUDY OF BONE DEGRADATION MONITORING USING NBPS	101
7.6 EFFECT OF CRACK LOCATION.....	106
7.7 EFFECT OF DENSITY VARIATION	109
7.8 EFFECT OF SKIN LAYER	113
7.9 NBPS CONFIGURATION WITH SKIN, MUSCLE AND FAT LAYER.....	119
7.10 CONCLUDING REMARKS.....	121
Chapter 8 PRACTICAL APPLICATIONS AND UTILITY.....	122
8.1 INTRODUCTION	122
8.2 MULTIFARIOUS APPLICATIONS OF NBPS AND ITS LIMITATIONS.....	122

Chapter 9 CONCLUSIONS AND RECOMMENDATIONS	125
9.1 INTRODUCTION	125
9.2 RESEARCH CONCLUSIONS AND CONTRIBUTIONS.....	126
9.3 FUTURE RECOMMENDATIONS	129
APPENDIX A PZFLEX PROGRAM TO DETERMINE THE ADMITTANCE SIGNATURES OF NBPS INSTRUMENTED HAND BONE IN PRISTINE AND DAMAGED CONDITION.....	130
APPENDIX B PZFLEX PROGRAM TO DETERMINE THE ADMITTANCE SIGNATURES OF NBPS INSTRUMENTED FEMUR WITH SKIN FOR DETECTING PHYSIOLOGICAL DECAY LIKE OSTEOPOROSIS AS WELL AS EVALUATE THE EFFECT OF VARIOUS PARAMETERS ON ADMITTANCE SIGNATURES....	140
APPENDIX C INVENTION DISCLOSURE.....	150
REFERENCES	151
PUBLICATIONS.....	164
CURRICULUM VITAE	166

LIST OF FIGURES

Figure 1.1: Schematic details of laboratory model of dental implants in polyurethane specimen	3
Figure 1.2: Monitoring changes in condition of bones using EMI technique.....	3
Figure 2.1: Direct piezoelectric effect.....	14
Figure 2.2: Converse Piezoelectric effect	14
Figure 2.3: Load cell cross-section assembled inside the surface of the prosthesis.....	15
Figure 2.4: Two dimensional lattice twinning	19
Figure 2.5: Lattice structure of Austenite.....	19
Figure 2.6: Twinned martensite	20
Figure 2.7: Detwinned martensite state.....	20
Figure 2.8: 1 D PZT-structure interaction modeling scheme.....	24
Figure 2.9: (a) Schematic of PZT-abutment-implant (superstructure).....	28
(b) Experimental set up implant/abutment/bone system	28
Figure 3.1: Non-bonded piezo system for pulse measurement	32
Figure 3.2: Pulse signal measured in non-bonded configuration	32
Figure 3.3: a) PZT patch bonded on rubber pad	33
b) Experimental set up	33
Figure 3.4: Pulse rate measurement by a rubber sheet based wrist tied assembly	34
Figure 3.5: Repeatability of pulse rate measurement using rubber-based wrist tied assembly.....	34

Figure 3.6: Scale Specimen with bolted screw	35
Figure 3.7: Repeatability of conductance signatures for the bonded piezo patch in pristine state	37
Figure 3.8: Conductance signatures for the bonded piezo patch with and without damage	37
Figure 3.9: Repeatability of conductance signatures for the non-bonded piezo patch in pristine state	38
Figure 3.10: Conductance signatures for the non-bonded piezo patch with and without damage.....	38
Figure 3.11: NBPS configuration with improved clamping	40
Figure 3.12: Conductance signatures in DBPS and NBPS configurations for specimen shown in Figure 3.11	40
Figure 3.13: Pristine and damaged conductance signatures in (a) NBPS and (b) DBPS configuration	41
Figure 4.1: NBPS-strip with PZT patch ready for clamping.....	45
Figure 4.2: Experimental set up for NBPS evaluation on artificial bone of human hand..	45
Figure 4.3: Conductance signature of piezo patch in NBPS mode on hand bone with clamps under different tightening conditions	48
Figure 4.4: Correlation of experimental signature peaks with theoretical values (shown in brackets).....	49
Figure 4.5: Comparison of DBPS and NBPS signatures for pristine bone	50
Figure 4.6: Repeatability of conductance signatures of NBPS for (a) Partially tightened clamp (b) Fully tightened clamp	52
Figure 4.7: (a) Specimen dipped in (MEK) solution to induce osteomalacia	54
(b) Degraded specimen.....	54

Figure 4.8: Comparison of conductance signatures for the laboratory bone in pristine and degraded condition for (a) NBPS (b) DBPS	55
Figure 4.9: (a) Healthy bone specimen (reference) (b) Osteoporotic bone specimen.....	57
Figure 4.10: Sensor diagnostics of (a) Reference (healthy bone) (b) Osteoporotic bone for the application of NBPS configuration	58
Figure 4.11: (a) Conductance signatures of healthy and osteoporotic bone using NBPS (b) Experimental signature peaks with theoretical frequency for healthy and osteoporotic bone (theoretical value shown in brackets)	60
Figure 4.12: Bones with artificial skin	
(a) Reference (healthy) bone with skin	62
(b) Osteoporotic bone with skin.....	62
(c) Reference (healthy) bone with skin instrumented with NBPS.....	62
(d) Osteoporotic bone with skin instrumented with NBPS.....	62
Figure 4.13: Repeatability check for NBPS in the presence of skin for	
(a) Reference (healthy bone) (b) Osteoporotic bone.....	63
Figure 4.14: Sensor diagnostics for application of NBPS on skin covered	
(a) Reference (healthy bone) (b) Osteoporotic bone.....	64
Figure 4.15: Comparison of conductance signatures of bones covered with skin with bare bones for (a) Reference (healthy) bone and (b) Osteoporotic bone.....	65
Figure 4.16: Comparison of conductance signatures of healthy and osteoporotic bones with skin for NBPS with fully tightened clamp	66
Figure 4.17: NBPS configuration test set up on live subject	68
Figure 4.18: Comparison of conductance signatures of live subject through NBPS configuration in different clamp positions.....	68

Figure 5.1: (a) Healthy bone with SMA clamping.....	71
(b) Osteoporotic bone with SMA clamping.....	71
Figure 5.2: Experimental set up	72
Fig 5.3: Repeatability of conductance signatures for SMA based	
(a) Partially tightened NBPS.....	75
(b) Fully tightened NBPS.....	75
Figure 5.4: Comparison of conductance signatures of open, partially tightened and fully tightened NBPS configuration with (a) SMA wire clamp (b) Jubilee clamps	76
Figure 5.5: Comparison of conductance signatures of healthy and osteoporotic bone with fully tightened NBPS configuration using (a) SMA wire clamping (b) Jubilee clamping.....	77
Figure 6.1: (a) Mechanical system	79
(b) Electrical circuit	79
Figure 6.2: Spring, mass and damper series combination representing healthy bone	84
Figure 6.3: (a) x and y for a standard series k-m-c system	84
(b) x and y for the experimental bone.....	84
Figure 6.4: Mechanical impedance of healthy bone in 70-100 kHz frequency range	
(a) Real part (x) vs frequency (b) Imaginary part (y) vs frequency	86
Figure 6.5: Mass in series with a spring and damper parallel combination representing ..86 osteoporotic bone	86
Figure 6.6: Mechanical impedance of osteoporotic bone in 70-95 kHz frequency range	
(a) Real part (x) vs frequency (b) Imaginary part (y) vs frequency	87
Figure 6.7: Mechanical impedance of healthy hand bone in 120-140 kHz frequency range	
(a) Real part (x) vs frequency (b) Imaginary part (y) vs frequency	88
Figure 6.8: Mechanical impedance of degraded hand bone in 120-140 kHz frequency range (a) Real part (x) vs frequency (b) Imaginary part (y) vs frequency	88

Figure 7.1: (a) FEM model of hand bone with DBPS and NBPS configuration	93
(b) Experimental hand bone in NBPS and DBPS configuration.....	93
Figure 7.2: FEM model of femur (see Figure 4.9 a for experimental bone).....	94
Figure 7.3: Comparison of conductance signatures of NBPS and DBPS instrumented on hand bone through (a) Numerical Analysis (b) Experimental analysis.....	98
Figure 7.4: Comparison of conductance signatures of NBPS instrumented on hand bone in open, partially and fully tightened configurations (a) Numerical (b) Experimental	100
Figure 7.5: Simulation of osteomalacia effect in numerical model	101
Figure 7.6: Conductance signatures of NBPS instrumented bone showing frequency peak shift due to physiological damage (osteomalacia) (a) Numerical (b) Experimental	102
Figure 7.7: FEM model of bone showing enlarged spherical cavity	103
Figure 7.8: Variation in conductance signature of piezo patch on hand bone with increase in size of spherical crack (a) NBPS configuration (b) DBPS configuration	104
Figure 7.9: Variation of RMSD with variance in crack size for NBPS and DBPS	105
Figure 7.10: Variation in conductance signature of NBPS instrumented hand bone with increase in size of spherical crack using NBPS configuration at a distance of (a) 62.5 mm from origin (b) 110 mm from origin	107
Figure 7.11: Comparison of conductance signatures of NBPS instrumented hand bone for crack at 62.5 mm and 110 mm from origin (a) 6 mm crack (b) 8 mm crack	108
Figure 7.12: FEM model of femur with (a) DBPS (b) NBPS	110

Figure 7.13: Variation in conductance signature with density variation in bone employing (a) DBPS configuration (b) NBPS configuration	111
Figure 7.14: RMSD with density variation in bone for both NBPS and DBPS configurations	112
Figure 7.15: Peak frequency shift with density change depicting osteoporosis.....	112
Figure 7.16: FEM model of femur bone with skin in (a) DBPS configuration (b) NBPS configuration	114
Figure 7.17: Comparison of NBPS and DBPS configuration for bone with skin	115
Figure 7.18: Comparison of conductance signatures employing NBPS configuration for healthy and osteoporotic bone (a) with skin (b) without skin	116
Figure 7.19: Variation in conductance signature with density variation in bone with skin layer employing (a) NBPS (b) DBPS	117
Figure 7.20: Variation of conductance signature with increase in skin layer thickness ..	118
Figure 7.21: Comparison of conductance signature of bone employing NBPS configuration in the presence of skin, muscle and fat layer	
(a) 1 mm thickness each of skin, muscle and human fat layer	120
(b) 3 mm thickness each of skin, muscle and human fat layer	120
Figure 8.1: Illustration of wearable NBPS type sensor	124

LIST OF TABLES

Table 2.1: Literature review based on EMI technique.....	25
Table 7.1: Properties of PZT patch and adhesive.....	96

LIST OF SYMBOLS

A	Cross-sectional area of the bone
B	Raw Susceptance
B_A	Active Susceptance
B_P	Passive Susceptance
c	Damping constant
D_{33}	Electric displacement over the surface of the PZT patch normal to axis '3'
d_{31}	Piezoelectric strain coefficient of PZT patch corresponding to axis '3' and '1'
E_3	Electric field along axis '3' of PZT patch
E	Young's modulus of elasticity of bone
F	(Effective force)
G	Raw conductance
G_A	Active Conductance
G_P	Passive Conductance
G_j^1, G_j^2	Reading 1 and 2 respectively corresponding to the j^{th} frequency
h	Thickness of piezo patch
I	Second moment of inertia
\bar{I}	Complex electric current
j	$\sqrt{-1}$
k	Spring constant
κ	Wave number
l	Half-length of the piezo patch
L_H	Half-length of the specimen
m	Mass of specimen

Q	Mechanical quality factor
S_l	Strain along axis '1'
T_l	Axial stress in the patch along axis '1'
\bar{T}	Complex tangent function
\bar{V}	Complex electric voltage
x	Real part of the mechanical impedance of the structure
x_a	Real part of the mechanical impedance of PZT patch
y	Imaginary part of the mechanical impedance of the structure
y_a	Imaginary part of the mechanical impedance of PZT patch
\bar{Y}	Complex electro-mechanical admittance
\bar{Y}_A	Active component of complex admittance
\bar{Y}_P	Passive component of complex admittance
\bar{Y}^E	Young's modulus of PZT patch at constant electric field
Z	Complex mechanical impedance of structure ($Z = x + yj$)
Z_e	Complex electrical impedance of structure
Z_a	Complex mechanical impedance of PZT patch ($Z_a = x_a + y_a j$)
$\bar{\epsilon}_{33}^T$	Complex permittivity of PZT patch along axis '3' at constant stress
ρ	Material density
ν	Poisson's ratio
δ	Dielectric loss factor
η	Mechanical loss factor of PZT patch
ω	Angular frequency
φ	Phase lag of velocity with respect to the applied force
α	Clamping factor

LIST OF ACRONYMS

BSHM	Bio-medical Structural Health Monitoring
PZT	Lead Zirconate Titanate
EMI	Electro-Mechanical Impedance
SMA	Shape Memory Alloy
FRF	Frequency Response Function
SHM	Structural Health Monitoring
NBPS	Non-bonded Piezo Sensor
PVC	Polyvinyl Chloride
DBPS	Directly Bonded Piezo Sensor
FEM	Finite Element Modelling
ESP	Equivalent Stiffness Parameter
NDE	Non-Destructive Evaluation
ESG	Electrical Strain Gauge
SPR	Surface Plasma Resonance
CNT	Carbon Nano Tubes
FBG	Fibre Bragg Grating
PVDF	Polyvinylidene Flouride
CLR	Carbon Loaded Rubber
RT	Respire Trace
sEMG	Surface Electromyography
aMSS	Active Muscle Stiffness Sensor
NiTi	Nitinol
BMD	Bone Mineral Density
pQCT	Peripheral Quantitative Computed Topography
MRI	Magnetic Resonance Imaging

Al	Aluminium Strip
MEK	Methyl Ethyl Ketone
SME	Shape Memory Effect
SMP	Shape Memory Polymer
EDP	Effective Drive Point Impedance
SDOF	Single Degree of Freedom
CFA	Coupled Field Analysis